

Multi-UAV Convoy Protection: An Optimal Approach to Path Planning and Coordination

X. C. Ding, A. Rahmani and M. Egerstedt

Abstract—In this paper we study the problem of controlling a group of Unmanned Aerial Vehicles (UAVs) to provide convoy protection to a group of ground vehicles. The UAVs are modeled as Dubins vehicles flying at a constant altitude with bounded turning radius. We first present time-optimal paths for providing convoy protection to stationary ground vehicles. Then we propose a control strategy to provide convoy protection to ground vehicles moving on straight lines. The minimum number of UAVs required to provide perpetual convoy protection in both cases are derived.

I. INTRODUCTION

CONTROL and coordination of heterogeneous unmanned vehicles is one of the canonical problems and the key to success for many proposed unmanned missions. We explore this coordination in the framework of providing ground convoy protection for a group of UGVs (Unmanned Ground Vehicles), using a group of dynamically more capable UAVs (Unmanned Aerial Vehicles). From the early days, airplanes have been used to provide close air support or large-scale area surveillance for ground convoys in unknown and potentially dangerous environments. Wide spread use of UGVs to conduct tasks in these environments has necessitated the design of practical approaches to effectively control and coordinate multiple UAVs to provide coverage, surveillance, tracking and convoy protection for the UGVs (see, for example, [2], [6], [11], [12], [16], [24]).

These UAVs often use on-board cameras to conduct the aforementioned tasks. In many surveillance applications with small UAVs (for example [18], [19]), the motion of the camera is decoupled from that of the UAV using a gyro stabilized camera platform that keeps the camera pointing in the same direction regardless of the motion of the UAV. This approach provides the UAV with crisp images even with high frequency oscillations of the UAV itself. Hence, in this paper we make the assumption that the on-board camera always points down and as such, the UAV monitors a circular disk on the ground.

In this paper, we adopt an optimal approach for path planning and coordination of multiple UAVs to provide convoy protection to ground vehicles. We model the UAVs as Dubins vehicles flying at constant altitude. Limited ranges of sensors on board the UAVs, together with their kinematic constraints, might make it impossible to provide coverage to the ground vehicles with a single UAV. In this case, we are interested in finding the best path for individual UAVs so that they can

monitor the ground vehicles for the longest time, and then coordinate the UAVs in such a way that the ground vehicles are visible to at least one UAV at any given time. Figure 1 visualizes this concept.

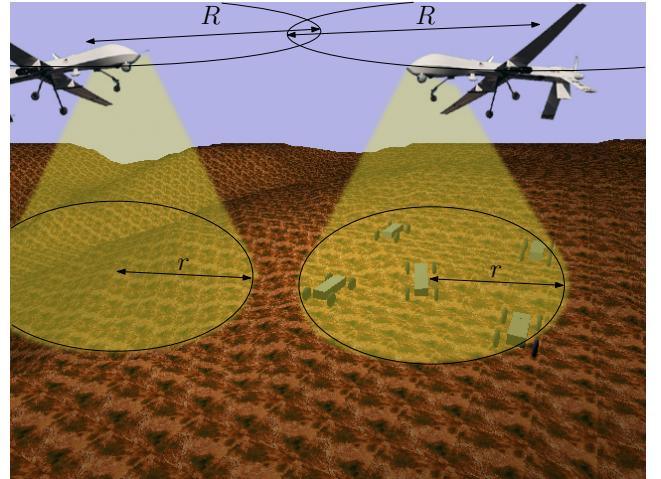


Fig. 1. UAVs providing convoy protection to UGVs. The UAVs are assumed to be kinematically restricted by their minimum turning radius R . The sensors on board the UAVs also have limited range and are assumed to be able to observe a disk of radius r on the ground.

A Dubins vehicle is a planar vehicle with bounded turning radius and constant forward speed. L.E. Dubins was the first to give a characterization of time-optimal trajectories for such a vehicle using geometric methods [8]. Shortest-path problems for Dubins vehicles have been since studied extensively (see [1], [4], [9] for example). A Dubins vehicle that can move backwards was studied by Reeds and Shepp [20], and the shortest-path problem for a Reeds-Shepp vehicle was further studied and classified by Souères and Laumond [23]. Walsh *et al.* [25] found optimal paths using quadratic cost functions for a Dubins airplane in $SE(2)$, $SO(3)$ and $SE(3)$. McGee *et al.* [17] obtained time-optimal paths for Dubins vehicles in constant wind. Dubins vehicles have moreover been used as a simplified model to describe planar motions of UAVs in [21]. Chitsaz *et al.* [5] extend the Dubins' model from $SE(2)$ to $SE(2) \times \mathbb{R}$ to account for altitude changes and gave a characterization of the time-optimal trajectories for this model based on the final altitude.

Optimal trajectories of a Dubins vehicle are often constructed using motion primitives (see [3], [10], [13] for example). For point-to-point minimum-time transfer problems, it has been shown that the optimal solutions are curves consisting of only three motion primitives: line-segments and circular

X.C. Ding, A. Rahmani, and M. Egerstedt are with the School of Electrical and Computer Engineering, Georgia Institute of Technology, Atlanta, GA 30308; Emails: {ding.amir,rahmani,magnus}@ece.gatech.edu. This research is supported by a grant from Rockwell Collins Advanced Technology Center.

arcs turning maximally to the left and to the right (see [8], [15], [22]). The optimal paths for the point-to-point minimum-time transfer problem are characterized by sequences of these three motion primitives. This paper shows that in the case of stationary convoy protection, time-optimal paths are characterized by sequence of only two motion primitives (maximally turning left and turning right) and do not include any line-segments.

This paper expands upon the results in [7], in which only the stationary convoy case was discussed. In this paper we address the problem of coordinated convoy protection using kinematically constrained UAVs for both stationary UGVs and UGVs moving on a straight line. We first consider the convoys as stationary and find the global optimal path for a single UAV to maximize the coverage time. Similar to many previous time-optimal path-planning work (e.g [4], [5], [17], [23], [22]), we use Pontryagin's Minimal Principle to derive optimal trajectories. We then show how to coordinate a group of UAVs to provide continuous coverage of the convoys and the minimum number of UAVs required to achieve continuous convoy protection for all time.

Next, we address ground convoys moving in a straight line and propose a control strategy for the UAVs so that their paths consists of alternating circular arcs. This control strategy guarantees periodical meet-up with the convoy, and it allows us to obtain a bound on the speed of the convoy so that continuous convoy protection can be provided by only one UAV for all time. If the speed of convoys is outside of this bound, we provide the minimum number of UAVs required to supply continuous convoy protection using this control strategy.

The rest of the paper is organized as follows: Section II formulates the problem. Section III address the problem in the case of stationary convoys. Section IV address the problem when the convoys are moving on a straight line, and Section V concludes the paper.

II. PROBLEM FORMULATION

The UAVs are modeled as Dubins vehicles flying at constant altitude with unit speed¹ and minimum turn radius of R . Therefore, we can write the kinematics of the UAVs as

$$\begin{cases} \dot{x} = \cos(\theta) \\ \dot{y} = \sin(\theta) \\ \dot{\theta} = \omega, \end{cases} \quad (1)$$

where x and y are the position of the UAV in the x - y plane at the altitude the UAV is flying, and ω is the angular velocity of the vehicle. The angular velocity is bounded by the inverse of the minimum turn radius R of the vehicle, i.e., $\omega \in [-\frac{1}{R}, \frac{1}{R}]$. We let the state of the system be given by $q(t) = [x(t), y(t), \theta(t)]^T$.

In this paper, we assume that the cameras on board the UAVs can monitor a disk of radius r on the ground (see Figure 1 for an illustration of this scenario). That is, we assume that the on-board camera is attached to a gyro and is always looking down, regardless of the bank angle of

the UAV. A gimballed camera system is commonly used in UAV surveillance applications (see for example [18], [19]). In addition, to simplify the problem, we consider ground convoys to be a point located at the centroid of the convoys in the x - y plane. Hence, we define successful convoy protection as being achieved when the centroid of the UGVs is visible to at least one of the UAVs at any time. Hence, convoy protection is provided by the UAV if the distance between the UAV and the centroid of the UGVs are less than or equal to r .

The disk of observation and its radius r certainly depend on the altitude of the UAV, but to ensure quality of observation and successful protection, cameras or sensors on board the UAV have narrower field of view than the UAV's turning radius in many cases, especially for cameras and sensors that carry out tasks using computer vision algorithms, which require certain level of image resolution. In these cases, $R > r$, and if the UGVs are stationary, then a single UAV is not capable of providing convoy protection to the ground vehicles indefinitely and a control strategy is needed to optimize the time in which convoy protection is achieved. This can be seen by drawing a circle of radius r using the position of the centroid of UGVs as the center. If there is only one UAV, then due to the fact that $R > r$, the UAV will eventually fly out of this circle no matter where it starts.

Note that in case of static convoys, if $R \leq r$, then the convoy protection problem is trivial since it can be solved by using a single UAV flying on a circular path of radius R with the center being the centroid of the ground vehicles. In this case, convoy protection is provided for all time using only one UAV.

In this paper we consider the problem of controlling and coordinating the UAVs to provide convoy protection for both stationary UGVs and UGVs moving on a straight line. In both cases we assume that $R > r$. We denote the *convoy circle* as a disk of radius r centered at the centroid of the UGVs. Using the convoy circle, it can be seen that convoy protection is achieved if at least one UAV is present inside the convoy circle at any time. Because of the kinematic constraint (turning radius R of the UAV), the UAVs are required to be coordinated so that they collectively provide continuous convoy protection while individual UAVs enter and leave the convoy circle.

III. OPTIMAL CONVOY PROTECTION FOR STATIONARY CONVOYS

A. Single UAV Time-Optimal Paths

First we consider the problem of using one UAV to provide convoy protection to some stationary UGVs for maximum amount of time, which is equivalent of finding the longest feasible path inside the convoy circle. We will determine both the optimal path for a single UAV starting at a fixed initial condition, and the optimal path if the UAV is allowed to pick the initial condition (position and heading) when entering the convoy circle.

Fix the origin of the x - y plane at the centroid of the UGVs. We then obtain a maximum-time optimal control problem with state constraint $x^2 + y^2 - r^2 \leq 0$ and input constraint $|w| \leq \frac{1}{R}$. Furthermore, it can be assumed that the UAV starts at a

¹The unit speed assumption is justified since the results presented in this paper describe paths, and these are invariant under different forward speed.

point on the state constraint boundary (convoy circle). This assumption does not limit generality of the result since if the UAV starts inside the convoy circle, we can use Bellman's Principle to obtain the optimal path for the UAV by integrating backwards in time.

To facilitate the analysis, it is useful to impose an extra terminal manifold constraint. Since the optimal solution always has the terminal state (henceforth denoted as the exit state) be on the boundary of the state constraint set (exiting the convoy circle), the terminal constraint of being on the convoy circle when exiting is enforced. To simplify the notation, we denote $q_T := q(T)$ and $[x_T, y_T, \theta_T] := [x(T), y(T), \theta(T)]$. Using these notations, the terminal manifold can be defined as the set of states that satisfy:

$$M(q_T) = x_T^2 + y_T^2 - r^2 = 0. \quad (2)$$

The optimal control problem can then be defined as:

Problem 3.1:

$$\min_{\omega(t)} J = \int_0^T -1 dt, \quad (3)$$

subject to the dynamics of (1) with a given initial condition $q(0)$, the input constraint

$$-\frac{1}{R} \leq \omega(t) \leq \frac{1}{R}, \quad (4)$$

the state constraint

$$x(t)^2 + y(t)^2 - r^2 \leq 0 \quad (5)$$

$$x(0)^2 + y(0)^2 - r^2 = 0 \quad (6)$$

and the terminal manifold constraint

$$M(q(T)) = x(T)^2 + y(T)^2 - r^2 = 0. \quad (7)$$

We henceforth denote this problem as $\Pi_{q(0)}$.

We exclude initial conditions that generate no paths entering the convoy circle. This occurs when the initial heading $\theta(0)$ points away from the convoy circle. The set of initial conditions Λ that are considered for the optimization problem are thus given by:

$$\Lambda = \{q = [x, y, \theta]^T : x^2 + y^2 = r^2, \text{ and } -\frac{\pi}{2} < \theta - \text{atan2}(y, x) < \frac{\pi}{2}\}. \quad (8)$$

We call set Λ the feasible entry set. For simplicity of notation, we assume that all angles are taken modulo 2π .

$\Pi_{q(0)}$ is an optimal control problem with both input and state inequality constraints. Optimal control problem with state inequality constraints are usually hard or impossible to solve explicitly. Fortunately, in this problem, due to the special structure of the state inequality constraint (5), there are only 2 points on the state trajectory where the constraint is active. These two states correspond to when the UAV is entering and exiting the convoy circle. Due to this special structure, we use an auxiliary state to handle the state constraint. Define $\xi(x^2 + y^2 - r^2)$ as an inverted Heaviside function:

$$\xi(x^2 + y^2 - r^2) = \begin{cases} 0 & : x^2 + y^2 - r^2 \leq 0 \\ 1 & : \text{otherwise.} \end{cases} \quad (9)$$

Define a new state τ as:

$$\dot{\tau}(t) = (x^2 + y^2 - r^2)^2 \xi(x^2 + y^2 - r^2), \quad (10)$$

The state of the UAV is then augmented as $\bar{q}(t) = [q(t), \tau(t)]^T$. Let us assume that $\tau(0) = 0$ and impose the terminal constraint that $\tau(T) = 0$. By imposing this constraint, and since $\dot{\tau}(t) \geq 0, \forall t \in [0, T]$, we have that $\dot{\tau}(t) = 0, \forall t \in [0, T]$. Hence,

$$\tau(t) = 0, \forall t \in [0, T]. \quad (11)$$

Note that the terminal constraint $\tau(T) = 0$ enforces the state inequality constraint (5). Using this auxiliary state τ , we are able to transform the state inequality constraint into an equivalent terminal constraint. When there is no ambiguity, we assume that the state constraint (5) is satisfied and we still call $q(t)$ the state trajectory.

The Hamiltonian for this optimal control problem is:

$$\mathcal{H} = -1 + \lambda_1 \cos \theta + \lambda_2 \sin \theta + \lambda_3 \omega + \lambda_4 (x^2 + y^2 - r^2)^2 \xi(x^2 + y^2 - r^2), \quad (12)$$

where $\lambda = [\lambda_1, \dots, \lambda_4]^T$ are the costates. The costates satisfy the following differential equations in the time interval $[0, T]$:

$$\dot{\lambda}_1 = -\frac{\partial \mathcal{H}}{\partial x} = -2x\lambda_4(x^2 + y^2 - r^2)\xi(x^2 + y^2 - r^2),$$

$$\dot{\lambda}_2 = -\frac{\partial \mathcal{H}}{\partial y} = -2y\lambda_4(x^2 + y^2 - r^2)\xi(x^2 + y^2 - r^2),$$

$$\dot{\lambda}_3 = -\frac{\partial \mathcal{H}}{\partial \theta} = \lambda_1 \sin \theta - \lambda_2 \cos \theta$$

$$\dot{\lambda}_4 = -\frac{\partial \mathcal{H}}{\partial \tau} = 0.$$

When the state constraint (5) is satisfied, the last term in the Hamiltonian (12) does not contribute since $\lambda_4(x^2 + y^2 - r^2)^2 \xi(x^2 + y^2 - r^2) = 0, \forall t \in [0, T]$, and thus the Hamiltonian becomes:

$$\mathcal{H} = -1 + \lambda_1 \cos \theta + \lambda_2 \sin \theta + \lambda_3 \omega. \quad (13)$$

The necessary optimality condition from the Pontryagin's Minimum Principle states that

$$\mathcal{H}(\bar{q}^*(t), \lambda^*(t), \omega^*(t), t) \leq \mathcal{H}(\bar{q}^*(t), \lambda^*(t), \omega(t), t), \quad \forall \omega(t) \in \left[-\frac{1}{R}, \frac{1}{R}\right], t \in [0, T], \quad (14)$$

where $\bar{q}^*(t)$ denotes the optimal augmented state trajectory, $\lambda^*(t)$ denotes the optimal costate trajectory corresponding to $\bar{q}^*(t)$, and $\omega^*(t)$ is the optimal control.

Using the necessary optimality condition (14) on the Hamiltonian equation (13), one can see that the optimal control $\omega^*(t)$ is a function of the costate $\lambda_3^*(t)$:

$$\omega^*(t) = \begin{cases} -\frac{1}{R}, & \text{if } \lambda_3^*(t) > 0 \\ \frac{1}{R}, & \text{if } \lambda_3^*(t) < 0 \\ \text{undetermined,} & \text{if } \lambda_3^*(t) = 0 \end{cases} \quad (15)$$

Thus, it can be seen that when $\lambda_3^*(t) > 0$, the optimal control is maximum turning right, and when $\lambda_3^*(t) < 0$, the optimal control is maximum turning left. When $\lambda_3^*(t) = 0$ for a finite time interval, then any control $\omega(t) \in [-\frac{1}{R}, \frac{1}{R}]$ satisfies the

Minimum Principle, and the finite time interval when this case arises is called a singular interval (for discussions on singular intervals for optimal control problems, see any standard text on optimal control, such as [14]). Hence, the optimal control is in the form of bang-bang (if there is no singular interval) or bang-off-bang (if there are singular intervals).

If there is a singular interval for $\Pi_{q(0)}$, then it is necessary that there exists a time interval $[t_1, t_2]$ such that, $\lambda_3(t) = 0$ and $\dot{\lambda}_3(t) = 0$ for all $t \in [t_1, t_2]$. For Dubins vehicles with dynamics specified in equation (1), singular intervals result in line segments as part of the optimal path. Line segments are usually part of the optimal paths for shortest-path (or minimum-time) Dubins vehicle problems. However, later in this section, we will show that line segments can not be part of the optimal path for $\Pi_{q(0)}$, and as a result the optimal control always switches between $\omega^*(t) = -\frac{1}{R}$ and $\omega^*(t) = \frac{1}{R}$.

Definition 3.1: For a state trajectory $q(t), t \in [0, T]$ satisfying the state constraint (5), if the costate trajectory $\lambda_3(t)$ and corresponding input $\omega(t)$ satisfies the control strategy (15), then $q(t)$ is referred to as a *Candidate Optimal Trajectory (COT)*.

Pontryagin's Minimum Principle states that being a COT is a necessary condition for being an optimal solution.

Assuming that a trajectory $q(t)$ is a COT but only its terminal state q_T is given, we will show that the entire trajectory $q(t)$, its corresponding costate trajectory $\lambda(t)$ satisfying the necessary optimality condition (14) and the control $\omega(t)$ satisfying the optimal control strategy (15) can all be uniquely determined from the terminal state q_T .

First, we note that, when the state constraint (5) is satisfied, i.e. the UAV is on or inside the convoy circle, the first three costate equations are independent from the augmented state, and they can be rewritten as

$$\begin{aligned}\dot{\lambda}_1 &= 0 \\ \dot{\lambda}_2 &= 0 \\ \dot{\lambda}_3 &= \lambda_1 \sin(\theta) - \lambda_2 \cos(\theta),\end{aligned}\quad (16)$$

with the terminal condition:

$$\begin{aligned}\lambda_1(T) &= \frac{\partial M}{\partial x}(x_T) = 2x_T\alpha \\ \lambda_2(T) &= \frac{\partial M}{\partial y}(y_T) = 2y_T\alpha \\ \lambda_3(T) &= \frac{\partial M}{\partial \theta}(\theta_T) = 0,\end{aligned}$$

where α is a constant Lagrange multiplier for the terminal manifold constraint (7).

Furthermore, being a minimum/maximum-time optimal control problem, the transversality condition gives that

$$\begin{aligned}\mathcal{H}|_{t=T} &= -1 + \lambda_1(T) \cos(\theta_T) + \lambda_2(T) \sin(\theta_T) \\ &\quad + \lambda_3(T) \omega(T) = 0,\end{aligned}$$

which implies that:

$$\alpha = \frac{1}{2(x_T \cos(\theta_T) + y_T \sin(\theta_T))}.$$

Thus, costate λ_1 and λ_2 are constant, and they can be given by

$$\lambda_1(t) = \frac{x_T}{x_T \cos(\theta_T) + y_T \sin(\theta_T)}, \forall t \in [0, T] \quad (17)$$

$$\lambda_2(t) = \frac{y_T}{x_T \cos(\theta_T) + y_T \sin(\theta_T)}, \forall t \in [0, T]. \quad (18)$$

Plugging (17) and (18) into (16), costate λ_3 is then given by the following differential equation:

$$\dot{\lambda}_3 = \frac{x_T \sin(\theta) - y_T \cos(\theta)}{x_T \cos(\theta_T) + y_T \sin(\theta_T)}, \quad (19)$$

with the initial condition $\lambda_3(T) = 0$.

Now, define the angle $\psi_T = \text{atan2}(y_T, x_T)$. Note that since q_T is an exit state, then $|\theta_T - \psi_T| < \frac{\pi}{2}$. If not, then q_T can not be an exit state since it points towards the convoy circle. This fact is illustrated in Figure 2.

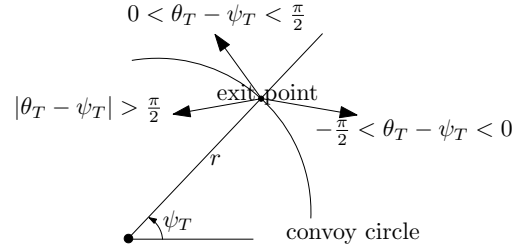


Fig. 2. Two possible and one invalid exit angles are shown on the same exit point. We can see that, in order for an exit angle to be valid, $|\theta_T - \psi_T| < \frac{\pi}{2}$ and the exit angle points away from the convoy circle.

Now, note that (19) can be simplified as the quotient of two inner-products, using ψ_T and the fact that $x_T^2 + y_T^2 = r^2$.

$$\begin{aligned}\dot{\lambda}_3(t) &= \frac{x_T \sin(\theta(t)) - y_T \cos(\theta(t))}{x_T \cos(\theta_T) + y_T \sin(\theta_T)} \\ &= \frac{\left\langle \begin{bmatrix} x_T \\ y_T \end{bmatrix}, \begin{bmatrix} \sin(\theta(t)) \\ -\cos(\theta(t)) \end{bmatrix} \right\rangle}{\left\langle \begin{bmatrix} x_T \\ y_T \end{bmatrix}, \begin{bmatrix} \cos(\theta_T) \\ \sin(\theta_T) \end{bmatrix} \right\rangle} \\ &= \frac{r \sin(\theta(t) - \psi_T)}{r \cos(\theta_T - \psi_T)} = \frac{\sin(\theta(t) - \psi_T)}{\cos(\theta_T - \psi_T)}.\end{aligned}\quad (20)$$

From (20), we see that

$$\dot{\lambda}_3(T) = \frac{\sin(\theta_T - \psi_T)}{\cos(\theta_T - \psi_T)} = \tan(\theta_T - \psi_T). \quad (21)$$

Since $|\theta_T - \psi_T| < \frac{\pi}{2}$, $\dot{\lambda}_3(T)$ can be determined completely by the exit state $q_T = [x_T, y_T, \theta_T]^T$ in the following way:

$$\dot{\lambda}_3(T) \begin{cases} > 0, & \text{if } \theta_T > \psi_T \\ < 0, & \text{if } \theta_T < \psi_T \\ = 0, & \text{if } \theta_T = \psi_T. \end{cases} \quad (22)$$

If $q(t)$ is a COT, then the corresponding control $\omega(t)$ satisfies the optimal control strategy (15). If $\theta_T = \psi_T$, we will show that the corresponding COT must be a line through the origin (in this case, $\lambda_3(t) = 0, \forall t \in [0, T]$). For the moment, let us assume that $\theta_T \neq \psi_T$, and thus $\dot{\lambda}_3(T) \neq 0$. In this case, since $\lambda_3(T) = 0$, $\lambda_3(t)$ must be non-zero and have the same

sign for a finite time interval (s, T) , $s < T$. Using the optimal control strategy (15), we have that:

$$\begin{cases} \omega(t) = -\frac{1}{R}, \theta(t) = \theta_T + \frac{1}{R}(T-t), \forall t \in (s, T) \\ \text{if } \lambda_3(t) > 0, \forall t \in (s, T) \\ \omega(t) = \frac{1}{R}, \theta(t) = \theta_T - \frac{1}{R}(T-t), \forall t \in (s, T) \\ \text{if } \lambda_3(t) < 0, \forall t \in (s, T). \end{cases}$$

Hence, we can obtain the analytical expression for $\lambda_3(t)$ in the interval (s, T) by integrating backwards.

$$\begin{aligned} & \lambda_3(t) \\ = & \lambda_3(T) - \int_t^T \dot{\lambda}_3(\xi) d\xi = 0 - \frac{\int_t^T \sin(\theta(\xi) - \psi_T) d\xi}{\cos(\theta_T - \psi_T)} \\ = & \begin{cases} \frac{R((\cos(\theta_T - \psi_T) - \cos(\theta(t) - \psi_T)))}{\cos(\theta_T - \psi_T)} & \text{if } \omega = \frac{1}{R} \\ -\frac{R((\cos(\theta_T - \psi_T) - \cos(\theta(t) - \psi_T)))}{\cos(\theta_T - \psi_T)} & \text{if } \omega = -\frac{1}{R} \end{cases} \\ = & \begin{cases} R \left(1 - \frac{\cos(\theta(t) - \psi_T)}{\cos(\theta_T - \psi_T)}\right) & \text{if } \omega = \frac{1}{R} \\ -R \left(1 - \frac{\cos(\theta(t) - \psi_T)}{\cos(\theta_T - \psi_T)}\right) & \text{if } \omega = -\frac{1}{R} \end{cases}, \\ & t \in (s, T), \text{ if } \theta_T \neq \psi_T. \end{aligned} \quad (23)$$

If $\theta_T \neq \psi_T$, it is possible to determine the length of time interval (s, T) , in which the costate $\lambda_3(t)$ contains the same sign. Then, the above process can be repeated until the entire trajectory of $\lambda_3(t)$ is obtained. This technique leads to the following lemma.

Lemma 3.1: For any terminal state q_T , a unique COT $q(t)$ and its corresponding input and costate history can be reconstructed. Furthermore, if $\theta_T \neq \psi_T$, then $q(t)$ is composed of maximally turning right or left curves, or combination of both at some switching times. If $\theta_T = \psi_T$, then $q(t)$ is a line that goes through the origin.

Proof: At a terminal state q_T , if $\theta_T > \psi_T$, then $\dot{\lambda}_3(T) > 0$. Hence, $\lambda_3(t) < 0$ for a time interval (s, T) , $s < T$. Since $q(t)$ is a COT and thus follows the optimal control strategy (15), then $\omega(t) = \frac{1}{R}$ and $\lambda_3(t) = R \left(1 - \frac{\cos(\theta(t) - \psi_T)}{\cos(\theta_T - \psi_T)}\right)$ on the time interval (s, T) . Let us denote (t_s, T) as the longest time interval such that $\lambda_3(t)$ is negative. Note that $\lambda_3(t)$ on the interval (t_s, T) is a convex function.

There are two possibilities. One is that $t_s = 0$, in this case the optimal control does not change and $\lambda_3(t) < 0, \forall t \in (0, T)$. The second possibility is that $t_s > 0$, and $\lambda_3(t_s) = 0$. In this case, tracing the costate $\lambda_3(t)$ backwards, it remains negative until when $\cos(\theta(t) - \psi_T) = \cos(\theta_T - \psi_T)$. Since $0 < \theta_T - \psi_T < \frac{\pi}{2}$, this condition only occurs when $\theta(t) - \psi_T = -(\theta_T - \psi_T)$. Therefore, we have

$$\theta(t_s) = -(\theta_T - \psi_T) + \psi_T. \quad (24)$$

Furthermore, t_s can be obtained explicitly as:

$$t_s = T - 2R|\theta_T - \psi_T|. \quad (25)$$

Since $\lambda_3(t_s) = 0$ and $\dot{\lambda}_3(t_s) = \frac{\sin(\theta(t_s) - \psi_T)}{\cos(\theta_T - \psi_T)} = -\tan(\theta_T - \psi_T) < 0$, we can conclude that $\lambda_3(t) > 0$ for a time interval (s, t_s) , $s < t_s$. Therefore, the optimal control based on (15) must switch at time t_s from $\omega = -\frac{1}{R}$ to $\omega = \frac{1}{R}$.

Now we repeat this process and continue backwards in time until the system hits the state constraint boundary (the convoy circle). The system may undergo many switches until hitting the convoy circle. Note that throughout this process, there is never a time t such that $\lambda_3(t) = 0$ and $\dot{\lambda}_3(t) = 0$. Hence there is no singular interval. The COT is unique since there is only one possible control decision at any instant of time that satisfies the optimal control law (15) (except at points in time when $\lambda_3(t) = 0$, but this is not a problem since $\lambda_3(t) = 0$ always takes place in a time interval of zero length).

If $\theta_T < \psi_T$ then the same analysis can be applied. In this case the control must switch at time t_s (which follows the same formula as equation (25)) from $\omega = \frac{1}{R}$ to $\omega = -\frac{1}{R}$.

If $\theta_T = \psi_T$, then the necessary condition for a singular interval is satisfied at the terminal time. if $\lambda_3(s) = 0$ for a time interval $s \in [t, T]$, then $\dot{\lambda}_3(s) = 0$, which implies that $\theta(s) = \theta_T$, $s \in [t, T]$ and $\omega(s) = 0$. Hence, the last segment of the COT is a line. Furthermore, there is no COT that connects a circular arc with a line, since if there is, then there is a non-singular interval $[t_1, t_2)$ connected with a singular interval $[t_2, T]$, $t_2 < T$. If the circular arc in the interval $[t_1, t_2)$ is maximally turning left, then $\omega = \frac{1}{R}$. However, in this case,

$$\begin{aligned} \lambda_3(t) &= R \left(1 - \frac{\cos(\theta(t) - \psi_T)}{\cos(\theta_T - \psi_T)}\right) \\ &= R(1 - \cos(\theta(t) - \psi_T)) > 0, t \in [t_1, t_2). \end{aligned}$$

Hence the optimal switching law (15) is violated. Similarly if the circular arc in the interval $[t_1, t_2)$ is maximally turning right, then $\lambda_3(t) < 0$ and $\omega = -\frac{1}{R}$. Both cases violate the necessary optimality condition, therefore a circular arc followed by a line can not be a COT. This implies that in the case when $\theta_T = \psi_T$, $\theta(t) = \psi_T, \omega(t) = 0, \forall t \in [0, T]$. Therefore, the COT is a line through the origin, and in this case, $\lambda_3(t) = 0, \forall t \in [0, T]$. ■

A direct consequence of Lemma 3.1 is that an optimal trajectory can not contain both a circular arc and a line segment. In addition, the COT can be either a line through the origin, or a curve consisting of circular arcs of radius R . Hence, if the optimal control is not constant, then it can only change between $\omega = -\frac{1}{R}$ and $\omega = \frac{1}{R}$, since there is no singular interval in that case. Henceforth in this paper, we use the term *switching* for the time instant when the control law switches between $\omega = -\frac{1}{R}$ and $\omega = \frac{1}{R}$. Furthermore, a switching point in a state trajectory is defined as the state when the controller switches.

For a number of terminal conditions q_T , the corresponding COTs are shown in Figure 3. For all of these terminal conditions, we fix the x - y coordinates of the terminal state at $[r, 0]^T$ (hence $\psi_T = 0$), but allow the exit angle θ_T to vary. The path in the x - y plane $[x(t), y(t)]$, costate $\lambda_3(t)$ and angle $\theta(t)$ are plotted from left to right.

To ease analysis of the optimal trajectories, it is useful to rotate the exit state q_T . It should be noted that, in this paper, we define rotation of the exit state of the UAV q_T by an angle β not as a rotation of $[x_T, y_T, \theta_T]^T$ in \mathbb{R}^3 , but rather as a rotation of $[x_T, y_T]^T$ by angle β in \mathbb{R}^2 with the addition that the heading θ_T is increased by β . Note that the costate equation $\lambda_3(t)$ is invariant under this rotation since it is a

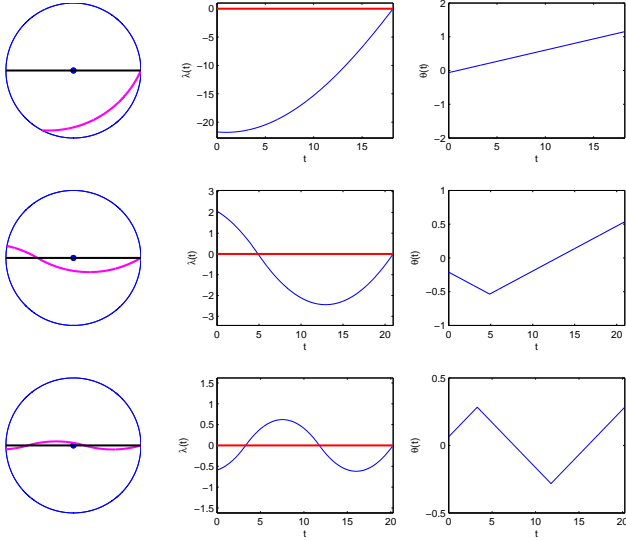


Fig. 3. A number of COTs are plotted for different exit angles θ_T resulting in different number of switchings. The left plots are the COTs in x - y plane, the middle plots are the costates λ_3 and the right plots are the angles $\theta(t)$. The first, second and third row correspond to the cases when this is 0, 1 and 2 switchings, respectively.

function of relative angle differences. Therefore, after the exit state is rotated by β , the corresponding x - y coordinates of the new COT is simply the rotation of the original COT by β in \mathbb{R}^2 .

Following this definition of rotation of the state of the UAV, let us rotate the exit state q_T by $-\psi_T$ to \tilde{q}_T , so that after rotation $\tilde{x}_T = r, \tilde{y}_T = 0, \tilde{\theta}_T = \theta_T - \psi_T$. Thus, after this rotation, $\psi_T = 0$ and $\tilde{\theta}_T \in (-\frac{\pi}{2}, \frac{\pi}{2})$ and $\tilde{q}_T = [r, 0, \tilde{\theta}_T]^T$. Next, tracing backwards in time and starting at T , we denote the i -th switching time as t_s^i . Furthermore, T is denoted as the 0-th switching time ($T = t_s^0$). Therefore, the switching time closest to T is denoted as the first switching time t_s^1 , et cetera. Under this switching time notation, $t_s^i < t_s^{i-1}$.

Using the analysis in the proof of Lemma 3.1, the switching angle $\tilde{\theta}(t_s^i)$ can be characterized as:

$$\begin{aligned} T - t_s^i &= 2R|\tilde{\theta}_T|i \\ \tilde{\theta}(t_s^i) &= \begin{cases} -\tilde{\theta}_T, & i \text{ odd} \\ \tilde{\theta}_T, & i \text{ even.} \end{cases} \end{aligned} \quad (26)$$

Using equations (26), the following lemma can be shown. This lemma is useful to obtain a simple and geometric law to determine optimal switching points.

Lemma 3.2: For any initial condition $q(0)$, all switching points of the optimal trajectory lie on the line passing through the origin and the exit point.

Furthermore, using the rotated coordinates (exit point rotated to $[r, 0, \tilde{\theta}_T]^T$), the x - y coordinates of the switching points can be determined by the following equation:

$$\begin{aligned} \tilde{x}(t_s^i) &= r - 2R \sin(\tilde{\theta}_T)i \\ \tilde{y}(t_s^i) &= 0. \end{aligned} \quad (27)$$

Proof: Rotate the optimal exit state to $[r, 0, \tilde{\theta}_T]^T$. If the

COT switches for i number of times ($i > 0$), then it is not a line and it must not contain a singular interval, hence $\tilde{\theta}_T \neq 0$. One can calculate the switching points by plugging in the end points and solve the state equations. If t_s^i refers to the i -th switching time, then the state $\tilde{q}(t)$ is in the following form in the time interval $[t_s^i, t_s^{i-1}]$:

$$\begin{aligned} \text{If turning left i.e.: } \omega(t) &= \frac{1}{R} : \\ \tilde{x}(t) &= \tilde{x}(t_s^i) + R \left(\sin(\tilde{\theta}(t)) - \sin(\tilde{\theta}(t_s^i)) \right) \\ \tilde{y}(t) &= \tilde{y}(t_s^i) - R \left(\cos(\tilde{\theta}(t)) - \cos(\tilde{\theta}(t_s^i)) \right) \\ \tilde{\theta}(t) &= \tilde{\theta}(t_s^i) + \frac{1}{R}(t - t_s^i), t \in [t_s^i, t_s^{i-1}] \\ \text{If turning right i.e.: } \omega(t) &= -\frac{1}{R} : \\ \tilde{x}(t) &= \tilde{x}(t_s^i) - R \left(\sin(\tilde{\theta}(t)) - \sin(\tilde{\theta}(t_s^i)) \right) \\ \tilde{y}(t) &= \tilde{y}(t_s^i) + R \left(\cos(\tilde{\theta}(t)) - \cos(\tilde{\theta}(t_s^i)) \right) \\ \tilde{\theta}(t) &= \tilde{\theta}(t_s^i) - \frac{1}{R}(t - t_s^i), t \in [t_s^i, t_s^{i-1}] \end{aligned} \quad (28)$$

Plug $t = t_s^{i-1}$ into the set of equations in (28) and solve recursively for all i , with the initial condition for $i = 0$ that $\tilde{x}(t_s^0) = \tilde{x}_T = r, \tilde{y}(t_s^0) = \tilde{y}_T = 0, \tilde{\theta}(t_s^0) = \tilde{\theta}_T$. The following switching-point expressions can be obtained for all i :

$$\begin{aligned} \tilde{x}(t_s^i) &= r - 2R \sin(\tilde{\theta}_T)i \\ \tilde{y}(t_s^i) &= 0. \end{aligned} \quad (29)$$

Since $\tilde{y}_T = 0$, therefore the exit point, switching points and the origin are on the same line for all COTs. Since COT is a necessary condition for an optimal trajectory, therefore this property holds for all optimal trajectories as well. ■

Again, using the rotated coordinates, equation (27) can be used to compute the required exit angle in order to produce a COT with i number of switchings. From (27), if a COT has i switchings, since $\tilde{x}(t_s^i) > -r$, then $R \sin(\tilde{\theta}_T)i < r$. Hence in order to have at least i number of switchings, the following condition must hold for the exit angle:

$$\tilde{\theta}_T < \arcsin \frac{r}{iR}. \quad (30)$$

If a COT has no switching, then $\tilde{\theta}_T \geq \arcsin \frac{r}{R}$.

Lemma 3.2 and equation (30) help to establish an important characterization of optimal trajectories as described in the next theorem.

Theorem 3.3: For any initial condition $q(0)$, the optimal trajectory of the UAV does not switch more than once.

Proof: We will prove by contradiction. We assume an optimal trajectory exists and it contains two or more switchings, and show by way of contradiction that it violates Bellman's Principle of Optimality.

Assume that $q(t)$ is the optimal trajectory. Therefore by Bellman's Principle of Optimality, all trajectory from $[t, T], t \geq 0$ must be optimal as well. Without loss of generality, we assume that $q_T = [r, 0, \theta_T]$. If this is not true, we can always rotate $q(t)$ so that it is true.

First assume that $\theta_T > 0$. If $q(t)$ has at least 2 switchings, then $\theta_T < \arcsin \frac{r}{2R}$. Now consider the first switching point, at t_s^1 , $x(t_s^1) > r - 2R \sin(\arcsin \frac{r}{2R}) = 0$. Therefore, the state at this switching time is $q(t_s^1) = [r - 2R \sin(\theta_T), 0, -\theta_T]^T$, where $r - 2R \sin(\theta_T) > 0$.

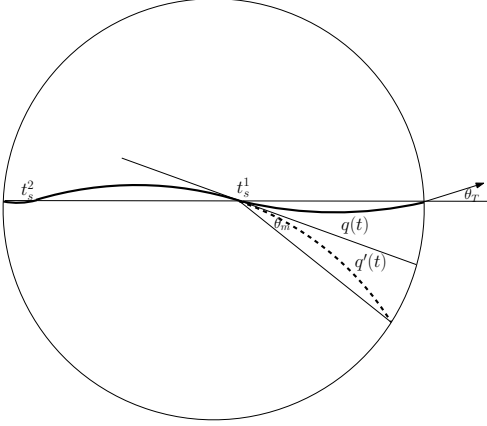


Fig. 4. Graph of example trajectory $q(t)$ and $q'(t)$. $q(t)$ is assumed to be an optimal trajectory that contains 2 switchings. $q'(t)$ is the same as $q(t)$ from time $t \in [0, t_s^1]$. However, it does not switch at time t_s^1 , hence contains only 1 switching. We show that in this case, $q(t)$ is shorter in length than $q'(t)$, so $q(t)$ can not be the optimal trajectory.

Consider that instead of switching at time t_s^1 to the left, the trajectory continues on arching towards the right (hence no switch). This new trajectory is denoted as $q'(t)$ and is only different from $q(t)$ after time t_s^1 . An example of the trajectories $q(t)$ and $q'(t)$ can be seen from Figure 4. Denote the angle between the tangent line at t_s^1 and the line connecting $[x(t_s^1), x_T]^T$ with $[y(t_s^1), y_T]^T$ as θ_m . The length of the line connecting $[x(t_s^1), x_T]^T$ and $[y(t_s^1), y_T]^T$ is $2R \sin(\theta_m)$. Using the cosine law, we have:

$$r^2 = (r - 2R \sin(\theta_T))^2 + (2R \sin(\theta_m))^2 + 2(r - 2R \sin(\theta_T))(2R \sin(\theta_m)) \cos(\theta_T + \theta_m)$$

Solving the above equation for $\sin(\theta_m)$ gives:

$$\sin(\theta_m) = f(\sin(\theta_T)),$$

where the function $f(a)$ is defined as:

$$f(a) = \frac{1}{2} \sqrt{\frac{h(a) + 2g(a)(r - 2Ra)}{6Rra - 8R^2a^2 - r^2 - R^2}}, \quad (31)$$

and $h(a)$ and $g(a)$ are defined as:

$$\begin{aligned} h(a) &= 16a^4R^2 + 6a^2r^2 - 4R^2a^2 - 20a^3Rr \\ &\quad + 4Rra - 2r^2 \\ g(a) &= \sqrt{(a^2 - 1)(4Ra^2 - r - 3ra)(4Ra^2 + r - 3ra)}. \end{aligned} \quad (32)$$

Note that $f(0) = 0$ and $f(\frac{r}{2R}) = \frac{r}{2R}$. Furthermore, after some careful algebra, one can see that $\frac{df}{da^2} < 0$ for $a = \sin(\theta_T) \in (0, \frac{r}{2R})$. Therefore $f(a) - a$ is a strictly concave function in this interval; and since $f(\frac{r}{2R}) - \frac{r}{2R} = 0$, $f(0) = 0$, one can conclude that $f(a) - a > 0$, if $a \in (0, \frac{r}{2R})$. Hence $\sin(\theta_m) >$

$\sin(\theta_T)$, and since $\theta_T \in (0, \frac{\pi}{2})$, we can finally conclude that $\theta_m > \theta_T$. Thus the right turning arc having length $2R\theta_m$ is longer than the left turning arc which has length of $2R\theta_T$. This implies that $q'(t)$ has a longer length inside the circle than $q(t)$. However this contradicts with Bellman's Principle of Optimality and therefore, $q(t)$ is not optimal.

The proof for $\theta_T < 0$ is exactly the same as above, except the curve is symmetric with $q(t)$ described above about the x-axis. If $\theta_T = 0$, then the unique corresponding COT is a line (as shown in Lemma 3.1) through the origin and there is no switching and it does not affect the theorem. ■

Since the optimal trajectory can only switch at most once, the number of COT that can be optimal is drastically reduced. It is then possible to construct optimal paths for any initial condition in the feasible set Λ . Similar to many other Dubins car path planning approaches (see [5], [13], [15], [23] for example), we can define motion primitives and use them to construct optimal paths. In Dubins car results for shortest path problem (see discussions about Dubins curves in [15] or [22]), the optimal paths consist of three motion primitives: maximum turning left, maximum turning right and going straight. However, now we show that a straight line segment is never part of an optimal trajectory for the static optimal convoy protection problem.

Corollary 3.4: Straight line segments can not be part of the optimal paths for Problem 3.1.

Proof: Lemma 3.1 states that the only case when straight line is part of a COT is when $\theta(t) = \psi_T, \forall t \in [0, T]$. Hence the COTs in this case are lines through the origin. However, a line through the origin is not an optimal path since there are 2 other COTs which are longer in length. One is initially turning left then switches to turning right at the point which is on the same line as the exit point and the origin. The other COT is exactly the same in length and it is turning right then left. ■

From Corollary 3.4, we can see that unlike the Dubins vehicle shortest-path problem, the optimal paths for Problem 3.1 do not contain line segments, and thus the motion primitive set does not contain the motion of going straight. Therefore, we define 2 motion primitives $\{\mathbf{L}, \mathbf{R}\}$, where \mathbf{L} and \mathbf{R} motion primitives turn the vehicle maximally to the left and right, respectively. Furthermore, since the optimal trajectory only switch once, there are only 4 possible sequences of the $\{\mathbf{L}, \mathbf{R}\}$ motion primitives, namely

$$\{\mathbf{L}, \mathbf{R}, \mathbf{LR}, \mathbf{RL}\}, \quad (33)$$

where \mathbf{LR} stands for turning left then right and \mathbf{RL} for turning right then left. There are two equivalent ways to determine the optimal switching point. The first one is geometric. As Lemma 3.2 states, the switching point must be on the same line as the origin and point of exit (this exit point can be determined by projecting the state either turning left or right until exiting the convoy circle). The second way is to check for the heading $\theta(t)$, which is required to satisfy equation (24) at the point of switching. Therefore, equation (24) provides a state-feedback optimal switching law for the control signal $\omega^*(t)$.

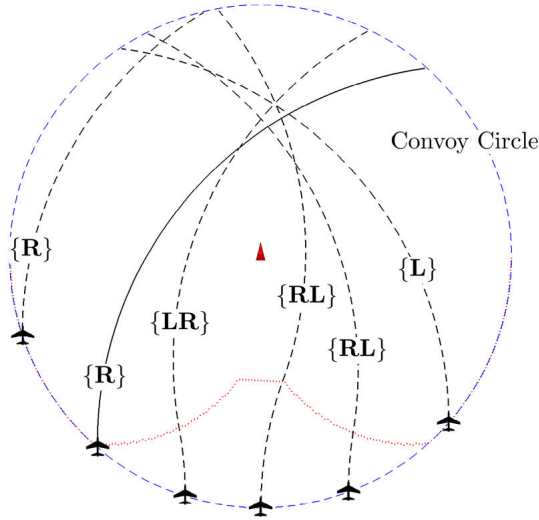


Fig. 5. A number of optimal state trajectories with initial heading $\frac{\pi}{2}$. The optimal switching points are plotted together to form the optimal switching surface. In this case, $R = 1.5r$. The dashed paths corresponds to optimal paths. If $x(0) \in (-\frac{r^2}{R}, 0]$, then **LR** is optimal. If $x(0) \in [0, \frac{r^2}{R})$, then **RL** is optimal. If $x(0) \in [\frac{r^2}{R}, r)$, then **L** is optimal. Otherwise, **R** is optimal. The optimal switching points are plotted together to form the optimal switching surface. The solid path corresponds to the initial condition that $x(0) = -\frac{r^2}{R}$. This path and the path where $x(0) = \frac{r^2}{R}$ are equal in length and longer than all other optimal paths with the same initial heading.

Since there are only 4 possibilities for the motion sequences in an optimal trajectory, it is easy to determine the global optimal path for any initial condition. A set of optimal paths for initial conditions with heading $\theta(0) = \frac{\pi}{2}$ are shown in Figure 5. Figure 5 also shows the optimal switching surface on which switchings are optimal. Observe that, for all cases when a switching is needed for the optimal trajectory, the switching point, the origin and the exit point are on the same line as described in Lemma 3.1.

By rotating the initial state until the initial heading is $\frac{\pi}{2}$, the switching surface in Figure 5 provides a control law which produces the optimal trajectory for any given initial condition. Now, we extend this result to address a perhaps more important problem: finding the optimal path inside the convoy circle with initial condition free to choose. Hence the problem of:

Problem 3.2:

$$\min_{q(0)} J^*(q(0)), \quad (34)$$

where $J^*(q(0))$ is the solution of Problem 3.1 ($\Pi_{q(0)}$), with the initial state $q(0)$.

Let the optimal initial condition be denoted by $q^*(0)$, hence:

$$q^*(0) = \arg \min_{q(0)} J^*(q(0)). \quad (35)$$

The optimal path with this initial condition will be referred to as a globally² optimal path. $q^*(0)$ will be called an optimal

²To clarify, the word *globally* is used here not within the context of local or global optimality. The solutions we obtained for Problem 3.1 are global optimal trajectories each corresponds to a fixed initial condition. A globally optimal path in this paper is defined as the longest path over all feasible initial conditions.

entry state. It is apparent that any rotation of this state around the origin is also an optimal entry state. Hence the globally optimal paths and optimal entry states are not unique. The set of optimal entry states, denoted by \mathbb{Q}^* , can be exactly determined by the following theorem.

Theorem 3.5: An optimal entry state $q^*(0)$ satisfies the equation:

$$(\theta^*(0) - \psi_T^*) = -(\theta_T^* - \psi_T^*). \quad (36)$$

To describe an optimal entry state geometrically, the optimal entry state, its corresponding exit state and the origin are always on the same line.

Proof: For any initial condition $q(0)$, assume that the exit state for its corresponding optimal trajectory $q(t)$ is at q_T^* and the exit state is rotated to $[r, 0, \theta_T]^T$. First, we have that $\theta_T \in (-\frac{\pi}{2}, \frac{\pi}{2})$. We focus on the case when $\theta_T \geq 0$, since COT with exit angle θ_T and COT with exit angle $-\theta_T$ are symmetric with respect to the x-axis. Furthermore, $\theta_T \neq 0$ since if it is true, then $q(t)$ is not an optimal trajectory. Thus, $\theta_T \in (0, \frac{\pi}{2})$.

Note the curve $q^*(t)$ in Figure 6. This curve corresponds to the smallest positive θ_T ($\theta_T = \arcsin(\frac{r}{R})$) without switching. It has the length of $2R \arcsin(\frac{r}{R})$. We will show that this curve is an optimal (longest) path in the convoy circle for any exit angle θ_T . By symmetry, if this is true, the curve with angle $\theta_T = -\arcsin(\frac{r}{R})$ is also the longest path in the convoy circle.

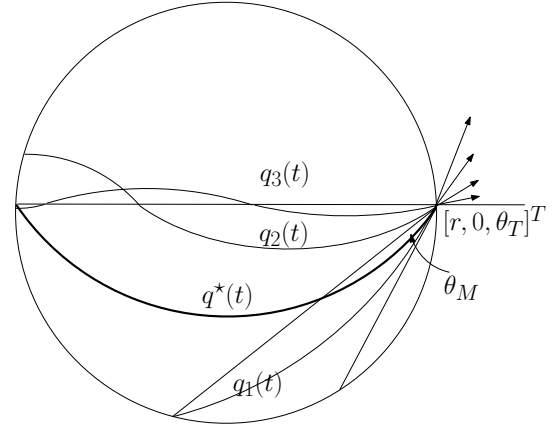


Fig. 6. Illustration of several COTs corresponding to different θ_T .

If $|\theta_T| < \arcsin(\frac{r}{2R})$, then the corresponding COT contains at least two switchings. Refer to $q_3(t)$ in Figure 6 for an example. Based on Theorem 3.3, this is not an optimal trajectory, and thus q_T^* can not be an optimal exit point.

If $|\theta_T| > \arcsin(\frac{r}{R})$, then the corresponding COT contains 0 switching (refer to $q_1(t)$ in Figure 6 for an example). Draw a line between $q_1(0)$ and $q_1(T)$ and denote the angle between this line and the tangent line at $q_1(T)$ to be θ_M . This line is shorter than the diameter since the diameter is the longest line inside a circle. Consequently, since this line has the length $2R \sin(\theta_M)$, we have $2R \sin(\theta_M) < 2r$, hence $\theta_M < \arcsin(\frac{r}{R})$, and the curve $q^*(t)$ having the arc length $2R \arcsin(\frac{r}{R})$ is longer than $q_1(t)$ with the arc length $2R\theta_M$.

Similarly, if $|\theta_T| \in [\arcsin(\frac{r}{2R}), \arcsin(\frac{r}{R})]$ (refer to $q_2(t)$ in Figure 6), $q_2(t)$ is always shorter than $q^*(t)$.

Since we have accounted for all possibilities of q_T^* which are the terminal conditions for the optimal trajectories starting from any arbitrary initial conditions. We can conclude that $q^*(0) = [-r, 0, \pm \arcsin(\frac{r}{R})]^T$ corresponding to terminal conditions $[r, 0, \mp \arcsin(\frac{r}{R})]^T$ are the optimal initial conditions which result in the longest state trajectories over the set of all initial conditions. Also since $\theta(0) = -\theta_T$, rotate the entry state back obtains equation (36). ■

From the proof of Theorem 3.5 we saw that all optimal entry states are rotations of the two states: $q(0) = [-r, 0, \arcsin(\frac{r}{R})]^T$ and $q(0) = [-r, 0, -\arcsin(\frac{r}{R})]^T$. By rotating these two states around the origin, the optimal entry state set \mathbb{Q}^* can be obtained in the following form:

$$\begin{aligned} \mathbb{Q}^* &= \{q = [-r \cos(\theta), -r \sin(\theta), \arcsin(\frac{r}{R}) + \theta]^T\} \\ &\cup \\ &\{q = [-r \cos(\theta), -r \sin(\theta), -\arcsin(\frac{r}{R}) + \theta]^T\}. \end{aligned} \quad (37)$$

An easy way to recognize a globally optimal path is to observe the fact that the entry state of a globally optimal path is always on the same line as the origin and the exit state.

B. Multi-UAV Convoy Protection

Due to kinematic constraint of the UAVs ($r < R$), it is impossible for one UAV to provide complete convoy protection for a group of UGVs. In this situation, multi-UAV coordination is required in order to successfully carry out convoy protection. The previous section laid out the groundwork to achieve optimal convoy protection by a group of UAVs. Theorem 3.5 characterized a set of optimal initial conditions that produces a set of globally time-optimal trajectory. It can be shown that these optimal trajectories not only specify a path inside the convoy circle, but also a path for a single UAV to come back to the convoy circle without changing direction. As shown in Figure 7, this path constitutes a circle of radius R and part of the path is a globally optimal path inside the convoy circle.

Definition 3.2: The circular paths of radius R entering and exiting the convoy circle at states satisfying equation (36) are referred to as the optimal convoy protection paths.

Figure 7 has shown three examples of optimal convoy protection paths. In the next lemma, we show that these paths each maximizes the ratio of time inside the convoy circle over the total travel time of the path.

Theorem 3.6: Over all simple closed paths of a single UAV, the optimal convoy protection paths each maximizes the ratio of the length inside the convoy circle over its total length.

Proof: Define the set of all simple closed path of the UAV as P . It is clear that the shortest paths over P is the set of all circular paths of radius R . Hence, if we define $P_R \subset P$ as the set of all circular path of radius R , and $L(q), q \in P$ as a

function that returns the total length of a path q , we have that $L(p) \leq L(q), \forall p \in P_R$ and $\forall q \in P$. Since $L(p) \geq 0, \forall p \in P$, we have that:

$$\frac{1}{L(p)} \geq \frac{1}{L(q)}, \forall p \in P_R \text{ and } \forall q \in P. \quad (38)$$

Now, let us define $L^i(p), p \in P$ as a function that returns the length of the path p inside the convoy circle, and P^* to be the subset of P_R where the entry state and exit state on the convoy circle satisfy equation (36). Due to Theorem 3.5, we have that if $p \in P^*$, the segment of path p inside the convoy circle is the maximum possible path inside the convoy circle. Hence, we have that

$$L^i(p) \geq L^i(q), \forall p \in P^* \text{ and } \forall q \in P. \quad (39)$$

Since $P^* \subset P_R$, and using (38), we have that:

$$\frac{L^i(p)}{L(p)} \geq \frac{L^i(q)}{L(q)}, \forall p \in P^* \text{ and } \forall q \in P. \quad (40)$$

This completes the proof. ■

Intuitively, an optimal convoy protection path maximizes the coverage ratio because it is the quickest path to come back to the convoy circle, always reenters optimally and repeats as a limit-cycle.

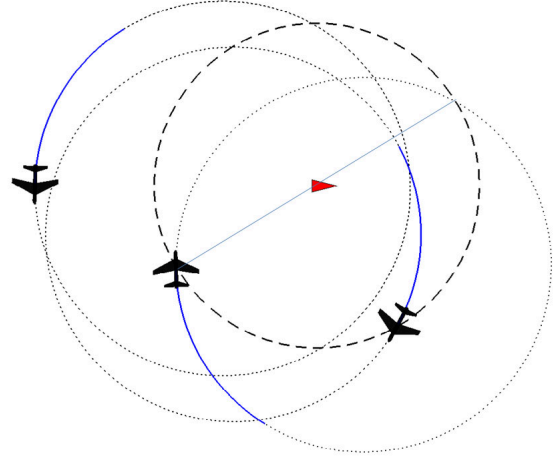


Fig. 7. Three optimal convoy protection paths are shown. They maximize the time spent inside the convoy circle over the time outside of the convoy circle. The smaller dashed circle is the convoy circle, and the larger dotted circles are optimal convoy protection paths. The solid curve is the past trajectories of the UAV. We can see that the key to coordinate the UAVs for optimal continuous convoy protection is to fly individual UAVs on optimal convoy protection paths, and space them out so that there is at least one UAV inside the convoy circle for all time.

To ensure that all the UAVs maximize their time providing convoy protection, their paths should be set to the optimal convoy protection paths such as the ones shown in Figure 7. In order to achieve successful convoy protection, it is required that the UGVs are visible to at least one UAV at all time. Thus, we can establish a lower bound on the number of UAV required to provide successful convoy protection for all time based on the length of the optimal convoy protection paths.

Corollary 3.7: Given the convoy circle of radius r for the UGVs and minimum turning radius R for the UAVs, the minimum number of UAVs needed to provide convoy protection for all time is:

$$N = \left\lceil \frac{\pi}{\arcsin(\frac{r}{R})} \right\rceil, \quad (41)$$

where $\lceil \cdot \rceil$ denotes the ceiling function.

Proof: Since the length of any optimal convoy protection path inside of the convoy circle is $2R \arcsin(\frac{r}{R})$, and the entire length of any optimal convoy protection path is always $2\pi R$, therefore it requires at least $\lceil \frac{\pi}{\arcsin(\frac{r}{R})} \rceil$ to cover the UGVs at all time. ■

Assume that there is N UAVs and they can start at an optimal initial condition $q^*(0) \in \mathbb{Q}^*$, the UAVs need to space themselves evenly in terms of the time entering the convoy circle. This can be achieved by slowing down and speeding up with respect to the other UAVs so that the i -th UAV enters the convoy circle at time $\frac{2\pi R}{N}i$. This strategy is possible since the optimal paths derived for this problem remain the same for UAVs of any speed (instead of unit speed).

IV. MOVING CONVOY PROTECTION

In this section we focus on a convoy protection strategy for moving UGVs. Again, we assume that the location of the UGVs are represented by their centroid as a point. Instead of being static, here we consider the case where this point is moving in a constant direction with a constant and bounded speed. Denote the speed of the UGVs as V_G . The UGVs are assumed to be moving in a constant heading of angle ϕ .

For the UAVs, we again normalize their speed to 1. Hence the UAVs follow the dynamics in equation (1) and their states are denoted by $[x, y, \theta]^T$. The UAVs are assumed to be capable of flying with faster speed than the UGVs (this agrees with current state of technologies in terms of speed of ground robots versus UAVs). Hence, we assume that $V_G \leq 1$.

Now, we propose a control strategy with a corresponding lower bound V_G^* so that if the speed of the UGVs is in this bound ($V_G \in [V_G^*, 1]$), then one UAV is guaranteed to provide convoy protection for all time.

Inspired by the motion primitives defined in the static convoy protection problem, we fix the motion of the UAV to a sequence of maximally left and right turns, i.e., $\mathcal{M} = \{\mathbf{L}, \mathbf{R}, \mathbf{L}, \mathbf{R}, \dots\}$ or $\mathcal{M} = \{\mathbf{R}, \mathbf{L}, \mathbf{R}, \mathbf{L}, \dots\}$. We assume that the UAV and UGVs are initially on top of each other; i.e., the initial x - y coordinates of the UGVs is $[x(0), y(0)]^T$. Now, we define the angle between the heading of the UGVs and initial heading of the UAV as β . Hence, $\beta = \phi - \theta(0)$. Again, to simplify notations, we assume that all angles are taken modulus 2π .

We switch the motion primitive between \mathbf{L} and \mathbf{R} every time the paths of UAV and UGVs intersect. With this control strategy, the path of the UAV and the UGVs intersect every time the UAV flies for a circular arc of angle 2β . An example of the trajectory of the UAV and the UGVs are shown in Figure 8. The initial motion primitive of the motion sequence \mathcal{M} depends on β . If $\beta \in [0, \pi)$, then the path of the UGVs

is to the left of the initial heading of the UAV and the first motion primitive is \mathbf{L} , otherwise, the first motion primitive is \mathbf{R} .

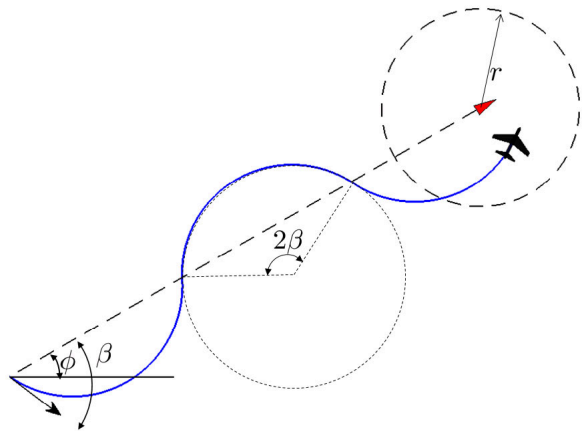


Fig. 8. Example trajectory of a UAV providing convoy protection for the UGVs with the proposed control strategy. The solid curve is the path of the UAV. The dashed line is the path of the UGVs. The dashed circle is the convoy circle. The angle of the circular arc for each motion primitive is 2β . In this case, $\beta \in [0, \frac{\pi}{2}]$.

In the following discussion, we focus on the case that $\beta \in [0, \pi)$ and the motion sequence is $\mathcal{M} = \{\mathbf{L}, \mathbf{R}, \mathbf{L}, \mathbf{R}, \dots\}$, because if $\beta \in (-\pi, 0]$, then the path of the UAV is symmetric to the path corresponding to the angle of $-\beta$.

It is desirable to control the UAV to meet the UGVs periodically. This goal can be achieved by carefully choosing the initial heading of the UAV based on the speed of the UGVs. The following lemma relates the speed of the UGVs with the desired initial heading of the UAV.

Lemma 4.1: Assume that the UGVs move with constant speed V_G and heading ϕ , and the UAV starts at the same position as the UGVs with the initial heading $\theta(0)$. $\beta = \phi - \theta(0)$. Assume that $\beta \in [0, \pi)$ and hence $\mathcal{M} = \{\mathbf{L}, \mathbf{R}, \mathbf{L}, \mathbf{R}, \dots\}$. Then if the UAV executes the proposed control strategy, and $V_G = \frac{\sin(\beta)}{\beta}$, then the UAV and the UGVs meet at the end of each motion primitive.

Proof: If the UAV executes the proposed control strategy, then it flies for a circular arc of angle 2β for each motion primitive in \mathcal{M} . Assume that the UAV meet with the UGVs at the end of each motion primitive. For each motion primitive, the UAV travels for a distance of $2R\beta$ and the UGVs travel for a distance of $2R\sin(\beta)$. Since the UAV is unit speed, we have $V_G 2R\beta = 2R\sin(\beta)$, and therefore $V_G = \frac{\sin(\beta)}{\beta}$. ■

Note that, if the UGVs travel with the same speed as the UAV, i.e. $V_G = 1$, then from Lemma 4.1, we have $\beta = 0$. In this case, the UAV will fly exactly on top of the UGVs.

Using Lemma 4.1, we can obtain the lower bound for the speed of UGVs to achieve perpetual convoy protection with the proposed strategy.

Theorem 4.2: Using the proposed control strategy, one UAV is sufficient to provide continuous convoy protection for all time, if V_G is bounded below by V_G^* , where

$$V_G^* = \frac{\sqrt{2rR - r^2}}{R \arccos(1 - \frac{r}{R})}. \quad (42)$$

Proof: Without loss of generality, we assume that the UAV and UGVs start at the origin and the heading of the UGVs is $\phi = 0$. If $\phi \neq 0$, We can always rotate the path of the UGVs so that $\phi = 0$. We first focus on the first motion primitive. Let us look at the positions of the UGVs and UAV after flying a circular arc of angle 2γ where $\gamma \in [0, \beta]$. Denote the x - y coordinates of the UGVs and the UAV as p_c and p_a , respectively. Note that p_c and p_a are both functions of γ , and they can be obtained after some algebra and trigonometry as

$$p_a(\gamma) = \begin{bmatrix} 2R \sin(\gamma) \cos(\beta - \gamma) \\ -2R \sin(\gamma) \sin(\beta - \gamma) \end{bmatrix}, \quad (43)$$

and

$$p_c(\gamma) = \begin{bmatrix} 2R \frac{\gamma}{\beta} \sin(\beta) \\ 0 \end{bmatrix}. \quad (44)$$

We denote the distance between the UAV and the UGVs as $d(\gamma)$, hence

$$d(\gamma) = \|p_a(\gamma) - p_c(\gamma)\|_2. \quad (45)$$

Note that $d(0) = d(\beta) = 0$, and $d(\gamma)$ is strictly concave in the interval $[0, \beta]$. Furthermore, $d(\gamma)$ is at the maximum exactly when $\gamma = \frac{\beta}{2}$. Thus, the distance between the UAV and the UGVs is at the maximum at the midpoint of the motion primitive.

The maximum distance between UAV and the UGVs can be computed as $d(\frac{\beta}{2}) = R(1 - \cos(\beta))$. If the UAV is sufficient to provide continuous convoy protection for the entire motion primitive, then we require that $d(\gamma) \leq r, \forall \gamma \in [0, \beta]$. This is true if $R(1 - \cos(\beta)) \leq r$. Since $\beta \in [0, \pi)$, we can obtain a bound on β :

$$\beta \leq \arccos(1 - \frac{r}{R}). \quad (46)$$

Note that $V_G = \frac{\sin(\beta)}{\beta}$, and the sinc function is strictly decreasing in $[0, \pi)$. Therefore, we have that $V_G \geq V_G^*$, where

$$V_G^* = \frac{\sin(\arccos(1 - \frac{r}{R}))}{\arccos(1 - \frac{r}{R})} = \frac{\sqrt{2rR - r^2}}{R \arccos(1 - \frac{r}{R})}. \quad (47)$$

This analysis can be applied to every motion primitive in the motion sequence \mathcal{M} . Thus, if $V_G \geq V_G^*$, then one UAV is sufficient to provide continuous convoy protection for all time. ■

When $V_G < V_G^*$, convoy protection cannot be provided with a single UAV and we need to coordinate multiple UAVs to provide perpetual convoy protection. We use a similar approach as the static convoys case to determine the minimum number of UAVs required. In this case, on the path of each execution of one motion primitive, there are two segments of the path when the distance between the UAV and the UGVs is less than or equal to r . Hence, convoy protection is provided by one UAV for two circular arcs of angle γ^* for each execution

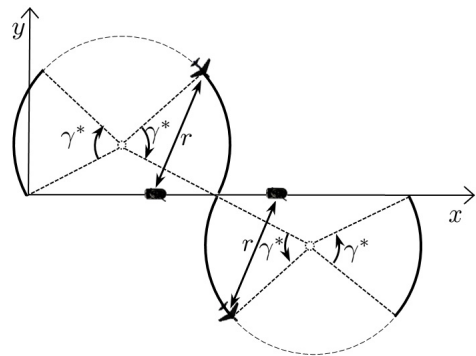


Fig. 9. For each execution of one motion primitive, there are two segments of the path corresponding to two circular arcs of angle γ^* , so that the distance between the UAV and the UGVs is less or equal to r when the UAV is on these segments. In this figure, the dashed curve is the path of the UAV, the solid curves are the segments of the path in which convoy protection is provided. The UAV and the convoys are drawn at the times when the UAV enters and exits these segments.

of one motion primitive, where $d(\frac{\gamma^*}{2}) = r$ and d is defined in equation (45). Refer to Figure 9 for an example.

Similar to the multi-UAV coordination approach in the previous section, we can use a timing strategy to schedule the UAVs such that, at any time, one of the UAVs is inside the convoy circle. First, note that the minimum number of UAVs required to provide continuous convoy protection can be obtained by the following corollary:

Corollary 4.3: Using the proposed control strategy, if $V_G < V_G^*$, then the minimum number of UAVs needed to provide continuous convoy protection for all time is $N = \lceil \frac{\beta}{\gamma^*} \rceil$, where $\lceil \cdot \rceil$ denotes the ceiling function. γ^* can be obtained by solving a non-linear equation $d(\frac{\gamma^*}{2}) = r$, using β obtained from V_G ($V_G = \frac{\sin(\beta)}{\beta}$).

Proof: Directly follows from the fact that, for each motion primitive, the length of the path in which one UAV stays inside the convoy circle is $2R\gamma^*$, while the length of the entire path for the motion primitive is $2R\beta$. ■

Figure 10 shows how one can schedule the UAVs to provide continuous convoy protection for all time. The key is to synchronize the position of the UGVs with individual UAVs at different times, so that when one UAV exits the convoy circle, there is at least one UAV inside the convoy circle and it is on the segment of its path in which the distance to the UGVs is less or equal to r .

V. CONCLUDING REMARKS

This paper studies the problem of providing convoy protection to a group of UGVs using UAVs. We assume that the cameras on board the UAVs are attached to gyros so that they always point down and project circles on the ground. The UAVs are kinematically restricted by their minimum turning radius and the sensors to provide convoy protection have limited range. In the case of stationary UGVs, this paper obtains optimal paths for one UAV to provide convoy protection for maximum amount of time. We also propose a

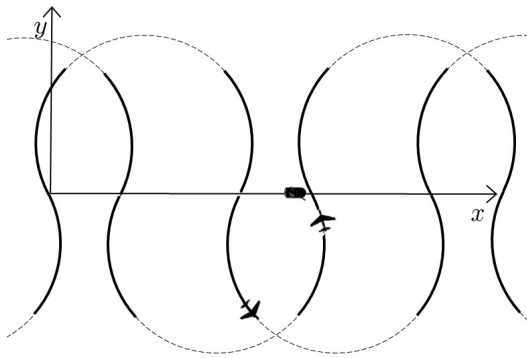


Fig. 10. Example of using two UAVs to provide continuous convoy protection using the proposed strategy. In this figure, the dashed curves are the paths of the UAVs, the solid curves are the segments of the paths in which convoy protection is provided. In this case, every time one UAV exits the convoy circle, the other UAV is inside the convoy circle. This is always true if $N = \lceil \frac{\beta}{\gamma \tau} \rceil = 2$ and the times when the UAVs synchronize with the UGVs are spaced out.

coordination strategy as well as optimal paths for multiple UAVs to provide continuous convoy protection for all time. The minimum number of UAVs required to achieve this task is derived. For the case of UGVs moving on straight lines with constant speed, we provide a control strategy that guarantees periodical meet-up with the UGVs, as well as a corresponding bound on the speed of the UGVs, so that if this bound is satisfied, then one UAV is capable of providing convoy protection for all time. If the speed of the UGVs is outside this bound, we propose a coordination scheme to be used with the proposed control strategy and obtain the minimum number of UAVs required to achieve continuous convoy protection with this strategy.

One possible extension of this work is to obtain the optimal paths of the UAVs if the UGVs obey Dubins or Reeds-Shepp car dynamics and are free to choose their path. Another possible direction is to find the optimal motion control of the cameras on board the UAVs, assuming that they can be actively controlled.

VI. ACKNOWLEDGEMENTS

This work was sponsored by a grant from Rockwell Collins Advanced Technology Center.

REFERENCES

- [1] P. Agarwal, T. Biedl, S. Lazard, S. Robbins, S. Suri, and S. Whitesides. Curvature-constrained shortest paths in a convex polygon. *Proc. ACM Symposium on Computational Geometry*, pp. 392-401, 1998.
- [2] R. Beard, T. McLain, D. Nelson, and D. Kingston. Decentralized Cooperative Aerial Surveillance using Fixed-Wing Miniature UAVs, *IEEE Proceedings: Special Issue on Multi-Robot Systems*, 94(7), pp. 1306-1324, July 2006.
- [3] C. Belta, A. Bicchi, M. Egerstedt, E. Frazzoli, E. Klavins, and G. J. Pappas. Symbolic planning and control of robot motion: State of the art and grand challenges. *IEEE Robotics and Automation Magazine*, Vol. 14, No. 1, pp. 61-70, 2007.
- [4] J. Boissonnat, A. Cérézo, and J. Leblond. Shortest paths of bounded curvature in the plane. *J. Intelligent and Robotic Systems*, Vol. 11, No. 1-2, pp. 5-20, 1994.
- [5] H. Chitsaz, S. M. LaValle. Time-optimal paths for a Dubins airplane, *IEEE Conference on Decision and Control*, pp. 2379-2384, Dec. 2007.

- [6] D. Cruz, J. McClintock, B. Perteet, O. Orqueda, Y. Cao, R. Fierro. Decentralized Cooperative Control - A multivehicle platform for research in networked embedded systems. *IEEE Control Systems*, Vol. 27, NO. 3, pp.58-78, 2007.
- [7] X.C. Ding, A. Rahmani, and M. Egerstedt. Optimal Multi-UAV Convoy Protection. *International Conference on Robot Communication and Coordination*, Odense, Denmark, Apr. 2009.
- [8] L. Dubins. On curves of minimal length with a constraint on average curvature, and with prescribed initial and terminal positions and tangents, *American Journal of Mathematics*, Vol. 79, pp. 497-516, 1957.
- [9] L. Dubins. On plane curves with curvature. *Pacific J. Math.*, Vol. 11, No. 2, pp. 471-481, 1961.
- [10] E. Frazzoli, M. A. Dahleh, and E. Feron. Maneuver-based motion planning for nonlinear systems with symmetries. *IEEE Trans. on Robotics*, Vol. 21, No. 6, pp 1077-1091, 2005.
- [11] A.R. Girard, A.S. Howell and J.K. Hedrick. Border Patrol and Surveillance Missions using Multiple Unmanned Air Vehicles, *IEEE Conference on Decision and Control*, pp. 620-625, Dec. 2004.
- [12] B. Grocholsky, J. Keller, V. Kumar and G. Pappas. Cooperative Air and Ground Surveillance: A scalable approach to the detection and localization of targets by a network of UAVs and UGVs. *IEEE Robotic and Automation Magazine*, Vol. 13, No. 3, pp. 16-26, 2006.
- [13] K. Hauser, T. Bretl, K. Harada, and J. C. Latombe. Using motion primitives in probabilistic sample-based planning for humanoid robots. *In Workshop on the Algorithmic Foundations of Robotics (WAFR)*, 2006.
- [14] D. E. Kirk. *Optimal Control Theory, An Introduction*, Dover Publications, 2004.
- [15] S.M. LaValle. *Planning Algorithms*, Cambridge University Press, NY, 2006.
- [16] J. Lee, R. Huang, A. Vaughn, X. Xiao, J. K. Hedrick, M. Zennaro, and R. Sengupta. Strategies of path-planning for a UAV to track a ground vehicle, *The Second Annual Symposium on Autonomous Intelligent Networks and Systems*, 2003.
- [17] T.G. McGee, S. Spry and J.K. Hedrick. Optimal path planning in a constant wind with a bounded turning rate. *AIAA Guidance, Navigation, and Control Conference and Exhibit*, San Francisco, California, Aug. 2005.
- [18] S. Morris and M. Holden. Design of Micro Air Vehicles and Flight Test Validation. *Proceeding of the Fixed, Flapping and Rotary Wing Vehicles at Very Low Reynolds Numbers*, pp.153-176, 2000.
- [19] M. Quigley, M. A. Goodrich, S. Griffiths, A. Eldredge, and R. W. Beard. Target Acquisition, Localization, and Surveillance using a Fixed-Wing, Mini-UAV and Gimbaled Camera. *International Conference on Robotics and Automation*, Barcelona, Spain, April 18-22, 2005.
- [20] J. Reeds and L. Shepp. Optimal paths for a car that goes both forwards and backwards. *Pacific J. Math.*, Vol. 145, No. 2, pp. 367-393, 1990.
- [21] K. Savla, E. Frazzoli, and F. Bullo. Traveling Salesperson Problems for the Dubins vehicle. *IEEE Trans. on Automatic Control*, Vol. 53, No. 6, pp.1378-1391, 2008.
- [22] P. Souères and J. Boissonnat. Optimal trajectories for nonholonomic mobile robots. *Robot Motion Planning and Control*, pp. 93-170. Springer, 1998.
- [23] P. Souères and J. Laumond. Shortest paths synthesis for a car-like robot. *IEEE Transactions on Automatic Control*, Vol. 41, No. 5, pp. 672-688, 1996.
- [24] S. C. Spry, A. R. Girard and J. K. Hedrick. Convoy protection using multiple Unmanned Air Vehicles: Organization and Coordination. *American Control Conference*, Portland, Oregon, Jun. 2005.
- [25] G. C. Walsh, R. Montgomery, and S. Sastry. Optimal path planning on matrix Lie groups. *IEEE Conference on Decision and Control*, Vol. 2, No. 14-16, pp. 1258-1263, 1994.



Xu Chu (Dennis) Ding received his B.S., M.S. and Ph.D. degree in Electrical and Computer Engineering from the Georgia Institute of Technology, Atlanta, in 2004, 2007 and 2009, respectively. He is currently a post-doctoral fellow at Boston University in the department of Mechanical Engineering. His research interests include optimal control of hybrid systems, coordination and control of multi-agent networked systems, and intelligent and persistent surveillance with a network of mobile agents.



Amir R. Rahmani received his Ph.D. in Aeronautics and Astronautics from the University of Washington, Seattle, WA, in 2008. Amir is a post-doctoral fellow at the School of Electrical and Computer Engineering, Georgia Institute of Technology, working on biologically inspired coordination and control of unmanned robotic teams. Amir's research focuses on understanding the role of the interconnection network in the performance of distributed dynamical systems as well as design of decentralized optimal estimation and control algorithms for teams of air,

land and space vehicles. Amir is also interested in enabling technologies for spacecraft formation flying.



Magnus Egerstedt (S'99-M'00-SM'05) was born in Stockholm, Sweden, and is an Associate Professor in the School of Electrical and Computer Engineering at the Georgia Institute of Technology. He received the M.S. degree in Engineering Physics and the Ph.D. degree in Applied Mathematics from the Royal Institute of Technology in 1996 and 2000 respectively. Dr. Egerstedt's research interests include hybrid and networked control, with applications in motion planning, control, and coordination of mobile robots, and he serves as Editor for Electronic

Publications for the IEEE Control Systems Society and Associate Editor for the IEEE Transactions on Automatic Control. Magnus Egerstedt received the ECE/GT Outstanding Junior Faculty Member Award in 2005, and the CAREER award from the U.S. National Science Foundation in 2003.